

## Control of 3D equilibria with resonant magnetic perturbations in MST

This content has been downloaded from IOPscience. Please scroll down to see the full text.

2015 Plasma Phys. Control. Fusion 57 104004

(<http://iopscience.iop.org/0741-3335/57/10/104004>)

View [the table of contents for this issue](#), or go to the [journal homepage](#) for more

Download details:

IP Address: 128.104.165.161

This content was downloaded on 03/09/2015 at 16:25

Please note that [terms and conditions apply](#).

# Control of 3D equilibria with resonant magnetic perturbations in MST

S Munaretto, B E Chapman, D J Holly, M D Nornberg, R J Norval,  
D J Den Hartog, J A Goetz and K J McCollam

Department of Physics, University of Wisconsin-Madison, 1150 University Avenue, Madison, WI 53706, US

E-mail: [smunaretto@wisc.edu](mailto:smunaretto@wisc.edu)

Received 28 January 2015, revised 9 April 2015

Accepted for publication 15 April 2015

Published 3 September 2015



CrossMark

## Abstract

To aid in diagnosis of 3D equilibria in the Madison Symmetric Torus, it has become necessary to control the orientation of the equilibria. In reversed field pinch experiments a transition to a 3D equilibrium is common with sufficiently large plasma current (and Lundquist number). Diagnosis of this state is hampered by the fact that the helical structure is stationary but with an orientation that varies shot-to-shot. A resonant magnetic perturbation (RMP) technique has been developed to vary controllably the orientation of the 3D equilibria and optimized to minimize the plasma wall interaction due to its use. Application of an RMP now allows alignment of the structure with key diagnostics, including Thomson scattering and an interferometer-polarimeter.

Keywords: reversed field pinch, resonant magnetic perturbation, 3D equilibrium

(Some figures may appear in colour only in the online journal)

## 1. Introduction

A resonant magnetic perturbation (RMP) is an external excitation of a mode resonant inside the plasma. The interaction between RMPs and the corresponding plasma tearing modes produces several effects that are studied in tokamaks, stellarators and reversed field pinches (RFP). RMPs can be used in stellarators, for example, to control and stabilize detached/radiative divertor plasmas [1, 2], or used to enhance the magnetic islands in the tokamak edge, generating stochasticity in the pedestal region that reduces the pressure gradient [3, 4]. In this way it is possible to suppress, or at least to mitigate, the heat flux from edge localized modes (ELMs) incident on the plasma facing components [3, 5–14]. Hence RMPs are a useful tool and are planned to be used in ITER [14, 15].

Some RFP devices are equipped with a large set of active coils to suppress resistive wall modes and error fields [16–18]. In these devices it is possible to use the active coils to produce RMPs. For example, in RFX-mod RMPs are routinely used to control tearing mode rotation to prevent strong plasma wall interaction and facilitate high plasma current [19].

One aspect of interest is the effect RMPs have on the dynamics of the tearing modes, particularly plasma rotation [20] and locking [21–24]. In this paper we describe the use of

RMPs in the Madison Symmetric Torus (MST) [25] to control both the orientation of 3D structures and the rotation of 2D plasmas.

MST is a toroidal device with major radius  $R = 1.5$  m and minor radius  $a = 0.52$  m. In the RFP configuration, many tearing modes with poloidal periodicity  $m = 1$  and toroidal periodicity  $n \gtrsim 2R/a$  are simultaneously present and nonlinearly interacting. At low plasma current ( $I_p \leq 0.3$  MA in MST) the perturbation energy is shared among several ( $m = 1, n$ ) modes; this configuration is called a *multiple helicity* (MH) state. In the MH state, the magnetic islands generated by the tearing modes overlap, leading to a high level of magnetic chaos in the plasma core. When the nonlinear interaction is reduced (either by dissipation or shear-suppression) the perturbation energy resides primarily in the innermost resonant mode and the magnetic configuration is called *quasi-single helicity* (QSH) [26, 27]. As the normalized amplitude of the dominant tearing mode exceeds a threshold of about 4% [28] the plasma magnetic axis merges with the O-point of the island corresponding to the dominant mode. This new axis is helically distorted with the periodicity of the dominant mode and this state is called the *single-helical-axis* (SHAx) state [28–30]. QSH and SHAx states are more likely at higher Lundquist number ( $S \sim I_p T_e^{3/2} / \sqrt{n_e} > 2 \times 10^6$ ) and therefore at higher plasma current ( $I_p \geq 0.4$  MA in MST) [31, 32].

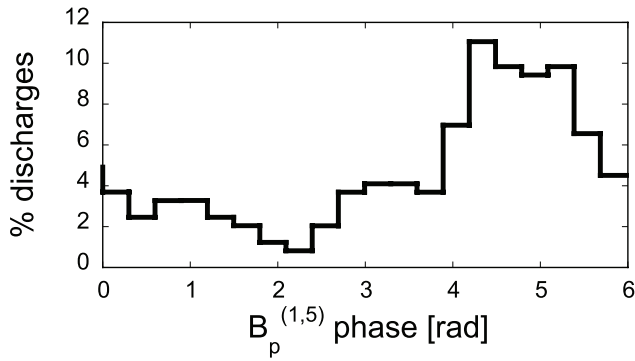


**Figure 1.** Probability to find the innermost resonant tearing mode locked at a particular poloidal phase angle at one toroidal location in MST during QSH state discharges. There is one locking event per discharge.

During the formation of QSH plasmas, as the dominant mode amplitude  $\mathbf{b}_{\text{mode}}$  grows, the plasma tends to decelerate and lock to the wall [33–35]. This behavior is ascribed to the induction of eddy current in the thick conducting shell surrounding the plasma [36, 37]. This eddy current has the same helicity as the core mode with a phase that lags the mode phase due to the finite shell inductance and resistance. This phase-lagged eddy current creates a magnetic perturbation at the mode resonant surface with current density  $\mathbf{j}_{\text{eddy}}$ . The resulting electromagnetic torque  $\mathbf{T}_{\text{em}} \propto \mathbf{j}_{\text{eddy}} \times \mathbf{b}_{\text{mode}}$  acts at the mode-resonant surface to oppose the rotation of the local plasma and the mode. As the plasma slows, the phase-lag is reduced, along with the braking torque. Eventually, the torque balance is sufficiently weak that torques due to small error fields can become the dominant force on the plasma, resulting in locking.

The shot-to-shot orientation of the locked helix is quasi-random with some favored orientations, as shown in figure 1. This asymmetry causes greater difficulty in analyzing data from advanced diagnostics, particularly the Thomson Scattering system [38] which samples the plasma minor radius at one toroidal location. For MH plasmas, the low fluctuation level and rapid rotation allow data to be interpreted in terms of small non-axisymmetric fluctuations superimposed on an axisymmetric equilibrium. Creating ensembles of measurements from locked QSH plasmas, however, requires creation of large numbers of reproducible discharges with an underlying bias in the sampled orientation. Control over this locking position facilitates creation of a higher quality data set with fewer discharges.

In this paper we demonstrate control of the orientation of 3D structures and the rotation of MH plasmas by applying a magnetic perturbation with a well-defined phase that is resonant with the innermost resonant tearing mode. Section 2 describes the active radial-field feedback system of MST and how it is exploited to generate RMPs. Section 3 demonstrates the use of an RMP to control the orientation of 3D structures with a description of the optimization of the control waveform in section 4. Section 5 discusses the observed plasma wall interaction associated with application of an RMP. Section 6 illustrates additional uses of RMPs, while section 7 highlights the limitation of the active feedback system in generating RMPs.

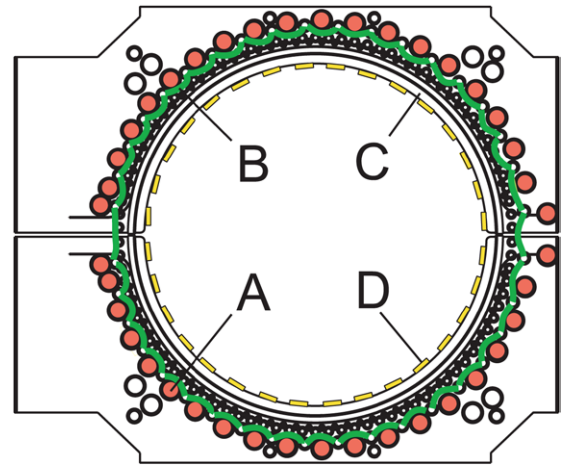


**Figure 2.** Cross-section of MST's poloidal gap, the vertical insulated cut of the shell. The inboard side of the torus is to the left. Shown in cross-section is: heavy copper primary turns in red (A); 30-turn field error correction saddle coils in green (B); the vacuum vessel (C); and in-vacuum radial field sense coils (D).

## 2. The active feedback system of MST

MST has a single poloidal flange with a gap to allow the poloidal magnetic field to enter the interior of the thick aluminum vacuum vessel (figure 2). The poloidal flange is pierced by forty insulated primary turns of heavy copper construction; these forty turns constitute the poloidal field primary winding for the 2 V-s iron core. An additional set of 38 small saddle coils (each consisting of 30 turns of #14 copper wire) provide radial error field correction on an irregularly spaced array. The radial field at the poloidal gap is measured by a uniformly-spaced set of 32 sense coils inside the vacuum vessel covering the gap. The field error correction coils are usually used to minimize the radial field at the gap sense coils. The gap error correction scheme is shown in figure 3.

The correction system hardware performs a minimization algorithm using matrix methods [39–41]. Signals from the 32 sense coils are integrated and input to a pair of analog matrix multiplier circuits (MM1 and MM2). MM1 performs a matrix calculation of the direct Fourier transform from poloidal angle to poloidal mode number. Each of the 32 output channels consists of a simple operational amplifier circuit which multiplies each input by a preselected weighting factor and yields the sum of these 32 weighted inputs. The weighting factors are the coefficients of a direct Fourier transform for poloidal mode numbers from  $m = 0$  to  $m = 16$ . If a pure spatial mode with amplitude  $V$  and mode number  $m$  is applied to MM1, the output on channel  $m$  is  $V \pm 2\%$  over a temporal frequency range from 0 to 150 kHz; no other channel has an output larger than  $V/100$  from 0 to 150 kHz. MM2 has a similar construction with 32 inputs and 38 outputs. It performs a matrix transform from Fourier space to correction coil location. The output signals are amplified and applied to the 38 saddle correction coils wound on the poloidal flange. Each amplifier uses an IGBT H-bridge which is pulse-width modulated at 25 kHz, so the frequency response is limited to several kHz. The correction coil inductances vary from coil-to-coil within a range of about

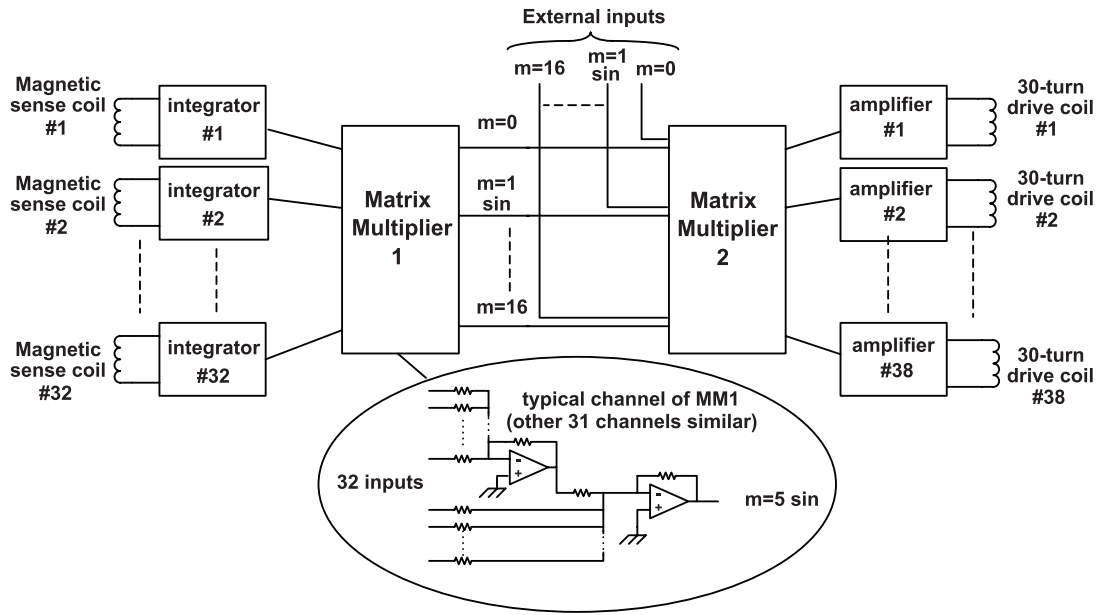


**Figure 3.** A schematic of the feedback-controlled error-field correction system for the poloidal gap on MST.

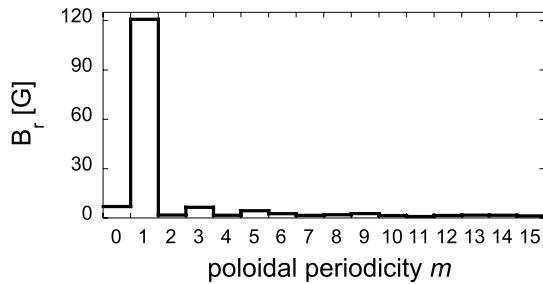


**Figure 4.**  $m$  radial mode spectrum during the application of a  $m = 1$  RMP.

40–120  $\mu\text{H}$ ; the amplifier's usual maximum output voltage of 300 V then limits the maximum slew rate of the output current. In addition, the amplifiers' output current is limited to 700 A to protect the IGBTs.

The weighting coefficients for MM2 were determined by driving each saddle coil separately in vacuum and measuring the response of the sense coils, yielding a  $32 \times 38$  matrix. This matrix was then inverted using Singular Value Decomposition. A simulation showed that while the weighting coefficients from this matrix inversion provided good correction of the radial field errors, they required unacceptably high currents with strong opposing polarity in adjacent coils. The weighting coefficients were therefore modified slightly to yield a smoother saddle coil current distribution, giving smaller saddle coil currents at the expense of a slight increase in field error.

In addition to the normal operation of minimizing the measured radial field, each input channel of MM2 (corresponding to a Fourier mode) is provided with an additional external input port. If a voltage is applied to one of these inputs, the system superimposes a field on the error-suppression field thus allowing the saddle coils to be used to create a radial field distribution with a selected mode spectrum, while suppressing

the other modes. Figure 4 demonstrates this capability of the field error correction system, where the  $m$  spectrum measured during the application of finite voltage to the  $m = 1$  input ports is shown. Due to the presence of the narrow (6 mm) poloidal gap in front of the active feedback coils, the toroidal  $n$  spectrum is broad, generating therefore both resonant and non-resonant error fields. Only the resonant ones have an effect on the tearing modes [42].

### 3. Orientation of 3D structures

The prospect of locking a rotating mode by applying an RMP through the poloidal gap at MST was previously demonstrated in MH plasmas [42]. The purpose of the present work is to extend this capability to lock QSH plasmas with a specified orientation.

Given the necessity of higher  $I_p$  and  $S$  for emergence of 3D equilibria, the discharges in this work, if not otherwise specified, have a plasma current  $I_p \geq 400\text{kA}$  and a central line averaged electron density  $0.5 \leq n_e \leq 1 \times 10^{19}\text{m}^{-3}$ . The present understanding of how the dominant core mode can rise to sufficient amplitude in MST plasmas involves decoupling the core resonant tearing mode from other resonant modes [43]. This coupling is typically provided by the  $m = 0$  modes resonant at the reversal surface in RFP plasmas. When the reversal surface is excluded from the plasma, the core mode can become decoupled allowing its amplitude to become much larger than the amplitudes of the other modes. The exclusion of the reversal surface is facilitated by operating MST with the toroidal field circuit opened so that  $B_t(a) = 0$ . Note that during normal operation where  $B_t(a)$  is negative, the innermost resonant tearing mode is  $(m = 1, n = 6)$  whereas it is  $(m = 1, n = 5)$  when  $B_t(a) = 0$ .

Figure 5 shows an example of a typical discharge with an RMP. The RMP is generated at the poloidal gap by adding

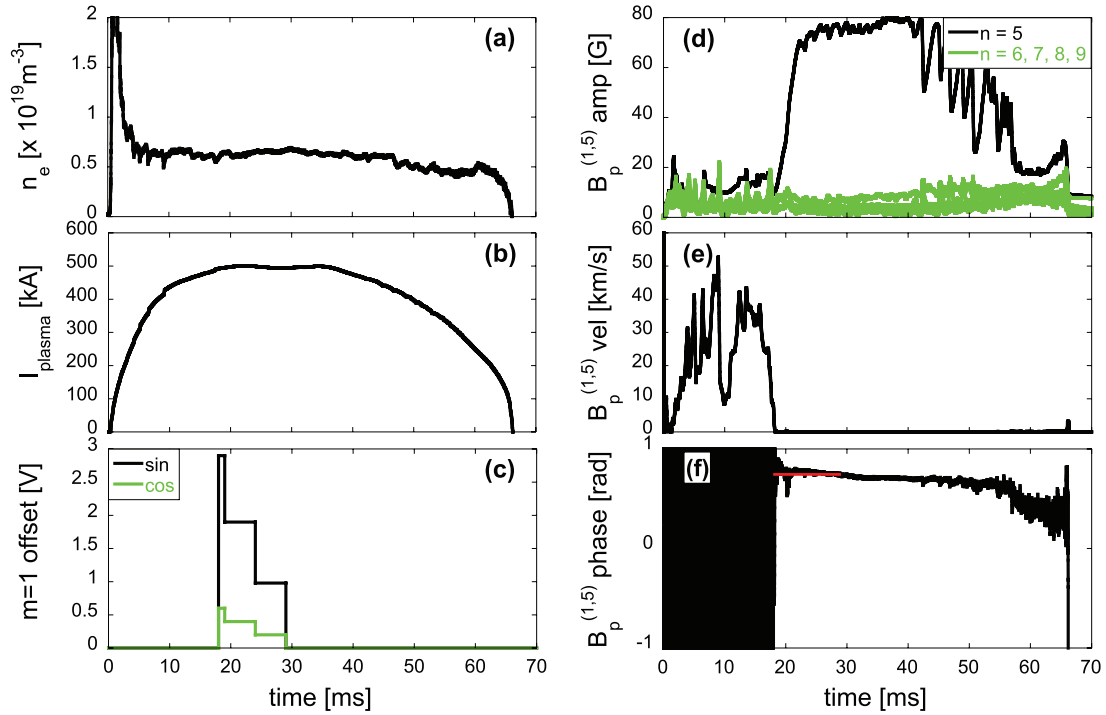


**Figure 5.** Example of typical discharge with the application of a RMP (1140207061). In (a) the time evolution of the electron density, (b) the plasma current, (c) the external demand to the  $m = 1$  part of the active feedback correction. (d)–(f) are amplitude, velocity and phase respectively of the  $n = 5$  poloidal component of the tearing modes. In green in (d) the time evolution of the amplitude of the  $6 \leq n \leq 9$  poloidal component of the tearing modes. The solid black data early in panel (f) correspond to a rapid rotation of  $2\pi$  radians of the mode and the y axis is clipped for plot clarity. The red line shows the desired locking phase.

an offset in the demand waveform of the active feedback system with  $m = 1$  sine,  $s$  and  $m = 1$  cosine,  $c$ , components, with the demand locking phase angle given as  $\delta = \arctan(s/c)$ . At  $t = 18$  ms a maximum offset of  $V_{\text{MAX}} = 2.9$  V in the sine component of the  $m = 1$  feedback system is requested and a maximum offset of  $V_{\text{MAX}} = 0.6$  V in the cosine component. The stepped temporal waveform of the required offset is intended to optimize the balance between the efficiency of the locking technique and the possible detrimental effects due to the plasma-wall interaction (PWI), which is discussed in section 4. The velocity of the  $m = 1$  tearing mode decreases until the mode locks. The desired locking phase angle of the mode (red) is overlaid on the  $B_p^{(1,5)}$  phase in panel 5(f). No macroscopic effects on the electron density, plasma current, dominant and secondary mode amplitudes or impurity content due to the applied RMP are observed.

The reproducibility of the innermost resonant tearing mode locking phase is quite good as seen in figure 6 where a histogram of the poloidal phase for locked QSH plasmas is shown. The histogram refers to a run day (about 100 discharges) where RMP locking was applied to lock the phase at  $\pi$  rad, in comparison with figure 1 where no RMPs were applied. Both days have comparable plasma parameters with  $0.5 \leq n_e \leq 1 \times 10^{19} \text{m}^{-3}$  and plasma current  $I_p \approx 500$  kA. The locking control is applicable to any desired phase angle, as seen in figure 7, where the open circles are the target angle and the red dots are the poloidal phase of the innermost resonant  $m = 1$  mode at the end of the application of the RMP. Each pair of dots corresponds to a single discharge.

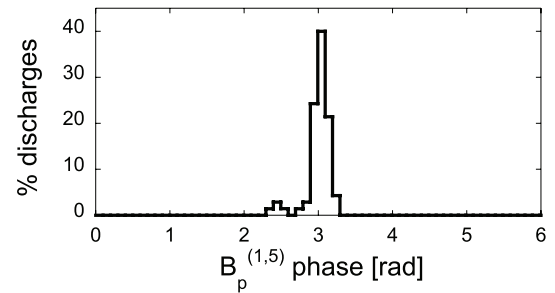


**Figure 6.** Distribution of the locking poloidal phase in a run day when a  $m = 1$  RMP is applied with a phase of  $\pi$  rad.

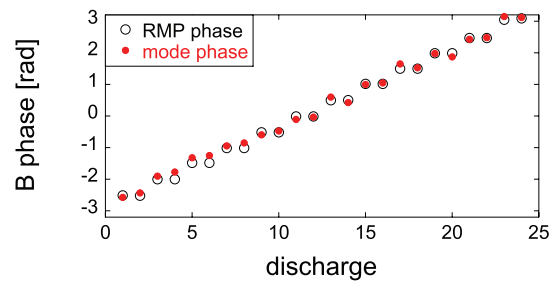


**Figure 7.** Locking poloidal phase for discharges with different RMP phase.

#### 4. Optimization of the applied RMP

There are two important parameters in the applied resonant magnetic perturbation waveform: the timing and the

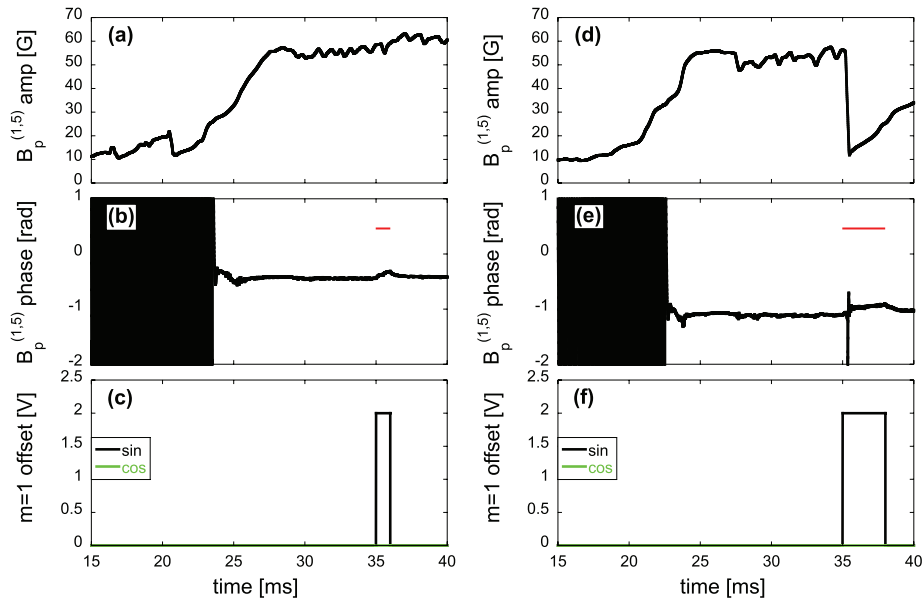


**Figure 8.** Examples of RMP applied when the plasma is already locked. The plots are the time evolution of: (a) and (d) amplitude of poloidal component of the core mode, (b) and (e) its phase and (c) and (f) the amplitude of the requested offset to the active feedback system. On the left a case with a RMP of  $B_r^{m=1} \simeq 120$  G applied for 1 ms (1130821026), on the right applied for 3 ms (1130821038). In (b) and (e) the red line corresponds to the requested locking phase.

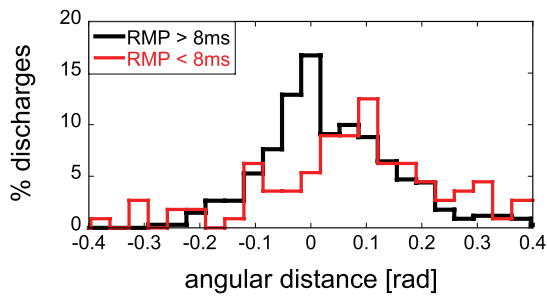


**Figure 9.** Histogram of the phase drift of the innermost resonant mode from 1 ms after the locking to the end of the plasma current flat top in case of RMP > 8 ms and of RMP < 8 ms.

amplitude. Several discharges during initial experiments were used to optimize these parameters.

#### 4.1. Timing

There were two initial strategies to determine the optimum timing of the RMP. The perturbation could be applied after the plasma was already locked to rotate it to the desired orientation where it would then re-lock. Alternatively, as shown earlier, it could be applied during rotation where the added perturbation would provide an additional external torque on the plasma to guide the rotating structure into the desired locking orientation.

The effect of applying a short ( $\Delta t \simeq 1$  ms) RMP when the mode is already locked is shown in the left panels of figure 8. The first row of the figure is the amplitude of the ( $m = 1, n = 5$ ) poloidal magnetic fluctuation, the second its phase and on the bottom the external demand applied. The result is a slight rotation of the mode towards the requested phase angle when the applied RMP is on. As soon as it is turned off, however, the phase drifts to the previous value. A longer ( $\Delta t \simeq 3$  ms)

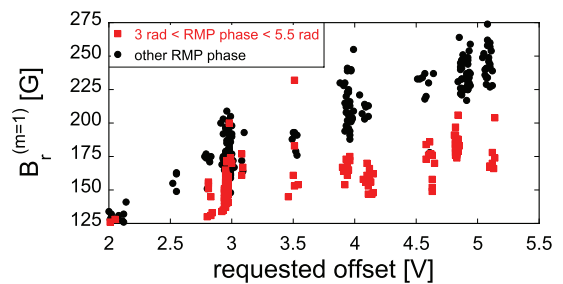


**Figure 10.** Amplitude of  $B_r^{m=1}$  measured by the sense coils at the poloidal gap as function of the offset requested to the active feedback. Points labeled in red deviate from linear dependence on the applied voltage due to the demand current exceeding a hardware limit in the feedback coil control.

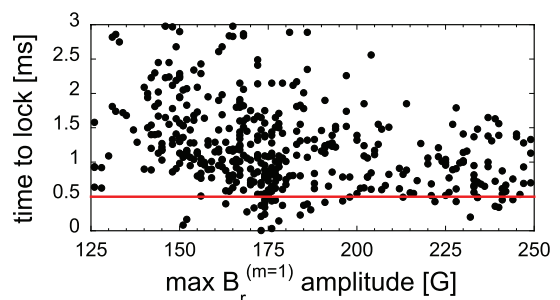


**Figure 11.** Time to lock as function of the amplitude of  $B_r^{m=1}$  measured by the sense coils at the poloidal gap.

perturbation (figure 8 on the right) does not improve the control. As shown in figure 5, a perturbation applied while the plasma is still rotating can successfully lock the mode at any desired phase. Most of the discharges where the plasma is in a QSH state lock between  $18 \leq t \leq 20$  ms, after the start up of the discharge at the same time the plasma current reaches its

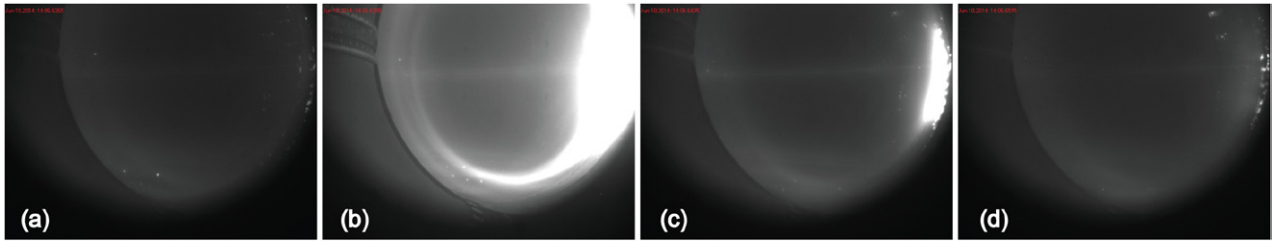


**Figure 12.** Time evolution of the PWI due to the application of a RMP. The data are from discharge 1140610079 characterized by  $I_p \simeq 500$  kA and RMP phase  $\simeq -2.7$  rad. In (a) the plasma is rotating, in (b) a RMP with  $B_r^{m=1}/B(a) \simeq 7\%$  is applied, in (c) the amplitude of the RMP is reduced to  $B_r^{m=1}/B(a) \simeq 3\%$  and in (d) there is no RMP but the plasma is still locked in the same position.

steady-state value. We apply the perturbation at  $t = 18$  ms to synchronize the RMP with the natural locking time.

We must also choose the duration of the applied RMP. The phase of the poloidal component of the innermost tearing mode at the end of the flat top tends to drift slightly in the co-current direction at the end of the plasma current flat-top, as can be observed in figure 5(f). This post-locking drift can be reduced by extending the duration of the applied RMP, at a lower amplitude. Figure 9 depicts a histogram of the difference between the phase at the end of the plasma current flat top relative to that at 1 ms after the locking for different RMP durations. When the perturbation is longer than 8 ms, 60% of the locked modes drift no more than 0.1 rad and 95% drift no more than 0.3 rad. When the applied perturbation is shorter than 8 ms the average drift is greater than 0.1 rad.

#### 4.2. Amplitude

One goal in this work is to apply the lowest amplitude perturbation that is able to lock the mode quickly enough to have the mode oriented in the desired position for most of the  $I_p$  flat top duration ( $\Delta t_{\text{flat top}} \simeq 20$  ms, see figure 5). The dependence of the  $m = 1$  RMP amplitude as a function of the offset applied is approximately linear as shown in figure 10, except for one subset of data (red squares) corresponding to an RMP with a phase between 3 and 5.5 rad. The deviation of the points is due to a hardware limitation for these particular RMP phases (see section 7). Note that it is possible to achieve  $B_r^{m=1} \geq 160$  G for any phase, corresponding to  $\approx 8\%$  of the magnetic field at the plasma surface.

Figure 11 shows the time it takes to lock the mode as a function of RMP amplitude. The *time to lock*,  $\tau_{\text{lock}}$ , is defined as the interval between the application of the resonant magnetic perturbation and the time when the velocity of the innermost resonant tearing mode drops below  $v_\phi = 100$  m  $s^{-1}$ . The scatter in the data is due to shot-to-shot scatter in the initial velocity and amplitude evolution of the  $n = 5$  mode. The red line highlights that to achieve  $\tau_{\text{lock}} \leq 0.5$  ms requires  $B_r^{m=1} \geq 150$  G and that raising the RMP amplitude above 180 G does not significantly reduce  $\tau_{\text{lock}}$ .

The three-step RMP waveform, as in figure 5(c), is designed in part to limit detrimental PWI which may lead to stronger impurity influx and a possible density excursion leading to premature plasma termination. A first step with a duration of 1 ms and a strong  $B_r$  is applied in order to slow initially the innermost tearing mode and possibly to lock it. To either

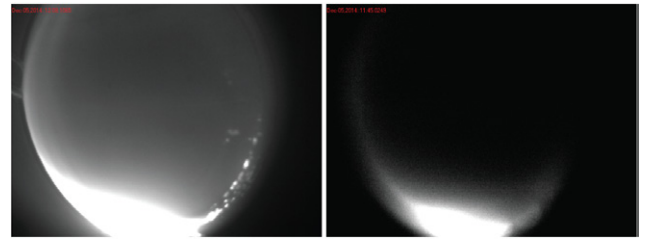


**Figure 13.** On the left visible and near infrared emission, on the right emission observed with a  $D_\alpha$  filter. Both the discharges have the same  $I_p$ ,  $n_e$  and both have an applied RMP of amplitude  $B_r^{m=1}/B(a) \simeq 9\%$  and phase  $\simeq -1.2$  rad.

continue slowing the rotating mode and ensure its locking or prevent it from drifting from the desired locked phase angle towards the next static error field in the machine, a weaker RMP is applied for the next 5 ms. Eventually an RMP with amplitude almost negligible in terms of PWI is applied for another 5 ms to hold the mode at the desired phase. The amplitude of the first step is usually of about  $B_r^{m=1} \simeq 160$  G, while the next two steps are 2/3 and 1/3 of the initial step amplitude.

## 5. PWI at the poloidal gap

Plasma-wall interaction during RMP application is monitored using a camera viewing the poloidal gap from a tangential porthole, toroidally displaced from the gap by  $75^\circ$ . The camera is sensitive in the visible and near infrared and has an integration time of 0.35 ms. Figure 12 depicts four frames from a single discharge: the first occurs when the plasma is still rotating, the second during the large-amplitude portion of a strong RMP ( $B_r^{m=1}/B(a) \simeq 7\%$ ), the third during the lower-amplitude portion ( $B_r^{m=1}/B(a) \simeq 3\%$ ) and the last when the plasma is locked to the wall after RMP application is over.

Despite strong emission, there are no indications of unusual erosion of material at the plasma boundary. For example, impurity emission observed by an array of monochromators is not altered by the application of a RMP. From the images of the PWI at the poloidal gap it is possible to confirm that the locking position can be controlled. An example is given in figure 13, where there are two discharges with the RMP phase  $90^\circ$  from the phase applied for the case shown in figure 12. This phase difference corresponds to the position of strongest emission in the images. The figure on the left shows all measured emission, while the one on the right has a  $D_\alpha$  filter passing

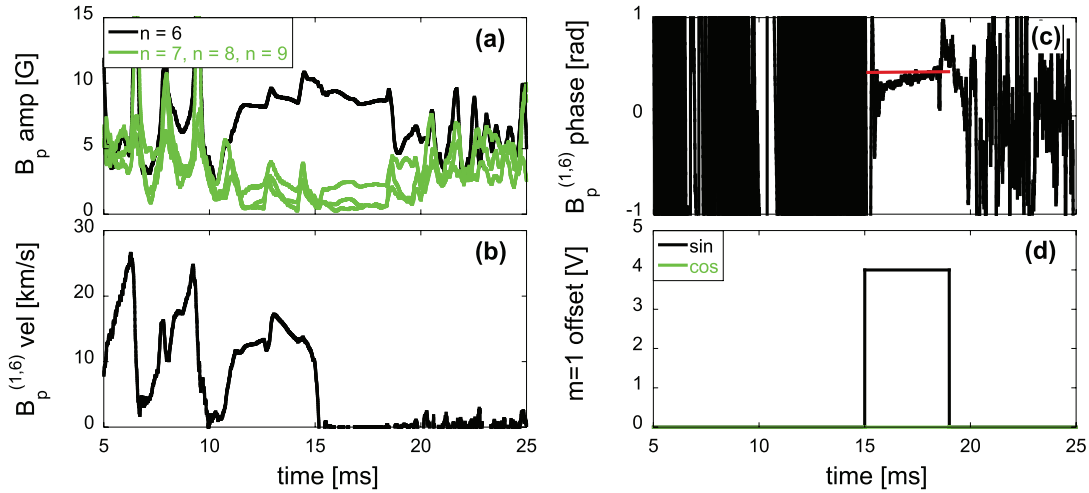


**Figure 14.** Example of a RMP applied during PPCD plasma showing (a) amplitude, (b) velocity and (c) phase of the poloidal  $m = 1, n = 6$  magnetic mode. Plot (d) shows the requested  $m = 1$  offset. PPCD is applied starting at 10 ms.

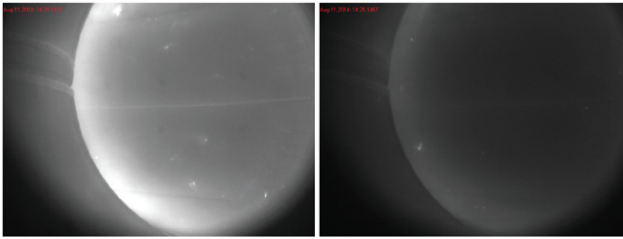


**Figure 15.** On the left visible and near infrared emission at the poloidal gap before the application of PPCD, on the right during the application of PPCD and a  $B_r^{m=1} \approx 170$  G ( $B_r^{m=1}/B(a) \approx 12\%$ ) RMP.

light at 656 nm. Since the filter passes only 16% of the light, the integration time on the right is extended to 0.7 ms and the emission in the figure, to be comparable with the unfiltered view, is divided by 0.32 to account for filter attenuation and the extended integration time. The similar emission pattern in the two images and the negligible emission detected using a carbon filter passing light at 464 nm (being carbon the material of the tiles constituting the poloidal limiter that protects the poloidal gap) suggests that most of the emission observed is from neutral deuterium. We hypothesize that plasma wall interaction due to RMP application creates strong local recycling.

## 6. Other applications of the RMP

The main purpose of developing a system to produce a RMP in MST was to control the orientation of the core helical equilibrium in QSH plasmas. Demonstrated success has prompted attempts at some other uses of the RMP.

### 6.1. Locking PPCD plasmas

In MST, an enhanced confinement regime is regularly achieved by controlling the current density profile through pulsed poloidal current drive (PPCD) [44–46]. By flattening the edge current profile gradient, the free energy available to

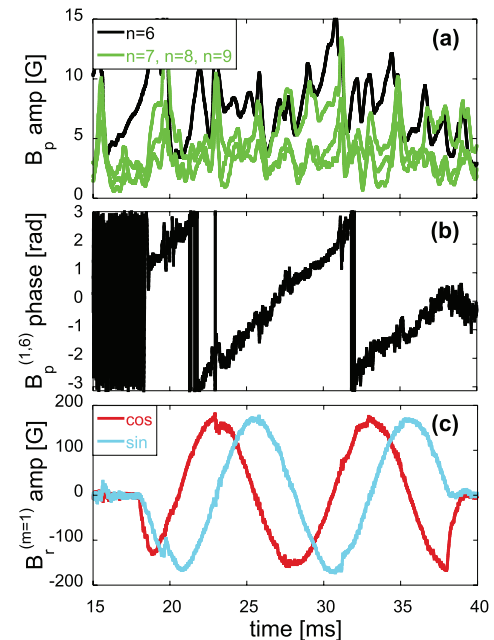


**Figure 16.** Application of a rotating RMP with a frequency of 100 Hz for a standard RFP discharge. (a) time evolution of the amplitude of the poloidal component of the core tearing modes, in black the  $m = 1, n = 6$  mode, in green the  $m = 1, 7 \leq n \leq 9$ ; (b) the phase of the poloidal component of the (1, 6) tearing mode; (c) the amplitude of the components of the  $m = 1$  RMP applied.

drive resistive tearing modes is reduced, leading to reduced transport. In this regime the presence of a dominant tearing mode at plasma current  $I_p \geq 400$  kA has been observed. Although the amplitude of the dominant tearing mode during PPCD plasmas is one order of magnitude smaller than in QSH plasmas, it is sufficient to couple to an external RMP that locks the mode. An example using a RMP to control the locking position is reported in figure 14.

The transition to the enhanced confinement is characterized by a strong reduction of the amplitude of most of the tearing modes. In this case it corresponds to the period  $12 \lesssim t \lesssim 18$  ms. The amplitude of the modes in panel (a) shows the

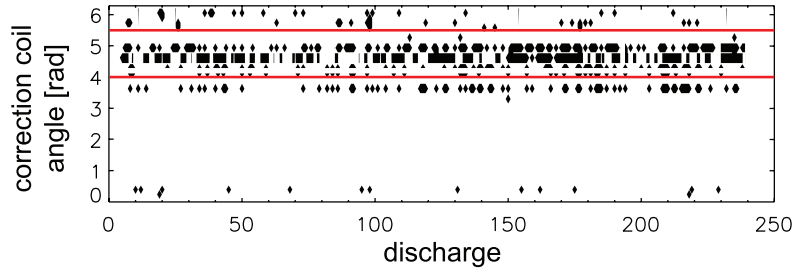


**Figure 17.** Saturation of the correction coils in discharges with  $I_p \simeq 500$  kA and  $B_r(a) = 0$  without applied RMP. The y axis is the angle of the correction coils, the x axis is discharge number and black points correspond to saturation of correction coils for that discharge in a time window between  $15 \leq t \leq 30$  ms. The two red lines highlight the most probable locking location area as suggested from the histogram in figure 1.

presence of a  $m = 1$ ,  $n = 6$  tearing mode (the innermost resonant  $m = 1$  mode when  $B_r(a) < 0$ ) with an amplitude that is significantly larger than the others. Plot (b) shows how the presence of a RMP can slow the mode rotation and plot (c) shows that the phase imposed through the RMP is maintained until the end of the enhanced confinement period.

The RMP in this case is longer and stronger than the RMP discussed above which was optimized for plasmas without current profile control. Larger RMPs are possible for PPCD plasmas without detrimental effects because plasma-wall interaction is already strongly reduced by PPCD. An example is reported in figure 15, where there is a snapshot of the visible emissivity during the application of the RMP in a PPCD discharge and the reduction of PWI is clear when compared with figure 12. The discharge reported is characterized by  $I_p \simeq 500$  kA, an applied RMP of amplitude  $B_r^{m=1} \simeq 170$  G and a locking position  $10^\circ$  displaced from the one in figure 13.

### 6.2. Low frequency rotation

The RMP system also is used to change the plasma rotation rate in multi-helicity plasmas. Prior attempts to control plasma rotation applying external fields on MST before the installation of the active feedback system were unsuccessful due to insufficient power coupled to the plasma [47]. Plasma rotation in an RFP induced by an applied RMP was achieved in RFX [48]. An  $m = 0$  RMP interacted with the  $m = 1$  modes through three-wave coupling. Plasma rotation through RMPs is routinely used in RFX-mod experiments by applying a rotating  $m = 1$  perturbation via a system of 192 saddle coils surrounding the vacuum vessel [19, 49, 50].

The position of the active feedback coils in MST limits their influence on structures in the plasma. Rotation control is achieved by rotating the poloidal phase of the RMP at a single toroidal location (the poloidal gap) and relying on the rigidity of the helical structure throughout the plasma. The results of a rotating RMP applied to a MH plasma with  $B_r(a) < 0$ ,  $I_p \simeq 400$  kA and  $n_e \simeq 0.6 \times 10^{19} \text{ m}^{-3}$  are reported in figure 16. The RMP is applied between  $18 < t < 38$  ms and the mode rotates at the frequency of the perturbation, performing 2 complete poloidal turns, thus proving the capability of reducing the rotating frequency of the innermost resonant tearing mode without locking it. Controlled RMP rotation is limited to a slower frequency than the natural rotation frequency of the

modes by the maximum frequency response of the active feedback system.

Attempts at rotating QSH plasmas revealed that the currents required to drive reliable rotation were beyond the capabilities of the existing active feedback system, as discussed in the next Section.

## 7. Hardware limitations

Control of plasma rotation and the locked orientation of 3D structures is inherently limited by the maximum current of the active feedback system. As stated in section 2, to protect the IGBTs in the correction coil amplifiers and the coils themselves, the system clamps the coil currents at about 700 A. Plasmas with  $I_p \geq 500$  kA typically require error correction current that exceeds this limit at particular coil locations, as seen in figure 17. When the demand exceeds the current limit, the active feedback system is unable to null the radial field. This residual radial field is sufficient to act as a static error field to which the modes lock. This over-current condition explains the preferred locking orientation of QSH plasmas; the coils whose current is clamped are located at the poloidal phase angle of the natural preferred locking area shown in figure 1. The demand current for applications such as rotating a QSH structure also exceed this current limit.

The effect of current clamping is shown in figure 18 on the left. The topmost plot is the time evolution of the  $B_p^{(1,5)}$  phase and the middle plot is the current in coil #36. The bottom plot shows in black the  $B_r$  measured by a sense coil located in front of the drive coil #36, in green the  $B_r$  produced in that position by the active feedback system and in red the  $B_r$  produced by the plasma. The saturation of coil #36, corresponding to the clamping shown between 18 ms and 27 ms in figure 18(b) indicated by the repetitive sawtooth of the current, gives rise to an error field of about  $B_r = 20$  G that persists up to the end of the discharge. In front of the non-saturated correction coils  $B_r \simeq 0$  G.

Current clamping is the reason that a lower  $B_r$  is produced at the same voltage requested for some angles in figure 10 and the possible reason for the impossibility to sustain the rotation during QSH. The latter is shown in figure 18 on the right, where the topmost plot is again the time evolution of the  $B_p^{(1,5)}$  phase in a discharge with a transition to QSH, the next the

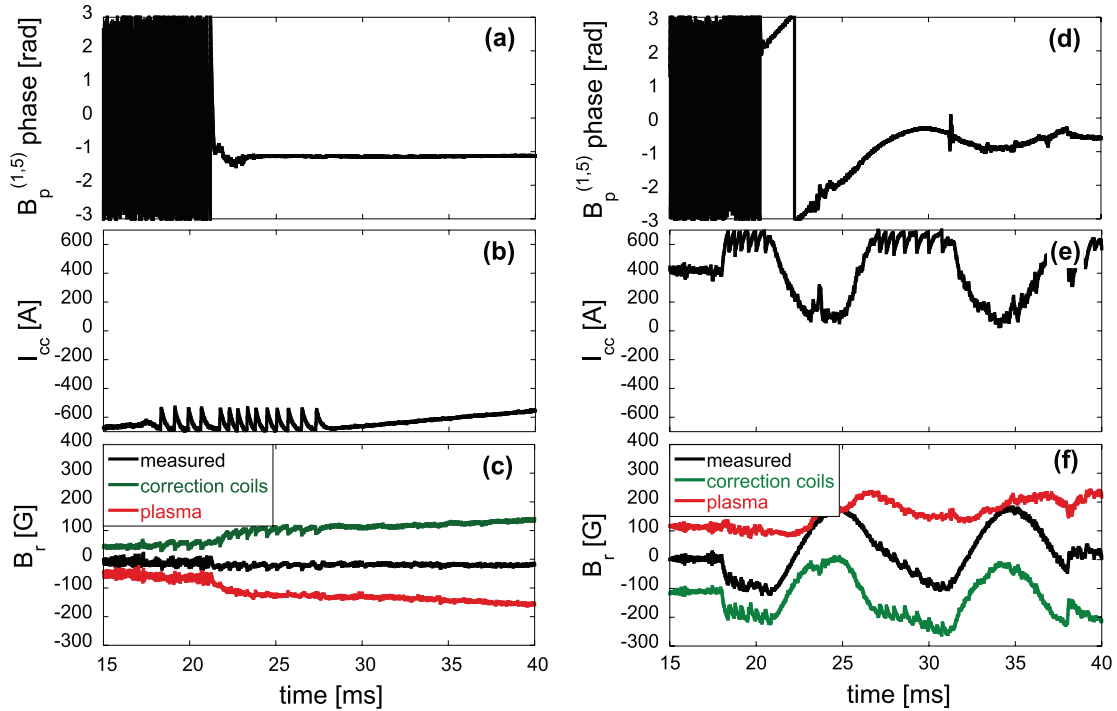


**Figure 18.** Effect of the correction amplifier clamping on the  $B_r$  measured at the poloidal gap. (a)–(c) a discharge at  $I_p \simeq 500$  kA and no RMP, (d)–(f) a discharge at  $I_p \simeq 400$  kA and rotating external RMP at a frequency of 100 Hz. (a) and (d) are the poloidal phase of the innermost resonant tearing mode. (b) and (e) the current in correction coil #36. Clamping is indicated by the sawtoothing of the current. Panels (c) and (f) are, in black the net  $B_r$  measured from a sense coil in front of the correction coil #36, in red the plasma component of  $B_r$ , and in green the component of  $B_r$  produced by the active feedback system.

current in the drive coil #36 and the last the components of the  $B_r$  measured by a sense coil located in front of the drive coil #36. This shows that when the coil saturates (at  $18 < t < 21$  ms and  $27 < t < 31$  ms) the active feedback system is not able to provide a sinusoidal RMP and as a consequence there is less control of the rotation of the mode. Also in this case the clamping is observed only in the usual set of correction coils.

Another problem that can be ascribed to the current clamping is that it is not possible to generate a pure  $m = 1$  perturbation, giving rise to a wider  $m$ -range perturbation. This was shown in figure 4, where the  $m$  spectrum during the application of a  $m = 1$  RMP is shown. Also stimulated are  $m = 0$ ,  $m = 3$  and  $m = 5$  components, but their amplitude is negligible compared to the  $m = 1$  and their presence does not influence the control on the  $m = 1$  modes.

## 8. Conclusions

Obtaining high-quality measurements of 3D structures in MST requires control of the orientation of the structure with respect to the diagnostic set. Using MST's active feedback system to create an RMP that guides the locking position of QSH plasmas during their formation has proven successful, with no evidence for enhanced impurity influx during the application of an RMP.

Besides the achievement of high-quality measurements, the capability to control the helix orientation is of more general importance. For example, two related and ongoing issues in fusion research are plasma-wall interaction and the ability

to exhaust power and particles flowing out of the plasma. One partial solution to these issues in the tokamak configuration is the divertor [51]. Implementation of a divertor in the RFP is challenging, but one possible approach [52] has been proposed that takes advantage of the naturally occurring 3D magnetic field topology like that described in this paper. But this approach requires control of the helix orientation, relative to fixed divertor components at the plasma boundary. Such control has been demonstrated in this paper.

## Acknowledgments

The authors would like to thank O Schmitz for his helpful comments and suggestions.

This material is based upon work supported by the US Department of Energy Office of Science, Office of Fusion Energy Sciences program under Award Number DE-FC02-05ER54814.

## References

- [1] Kobayashi M *et al* 2010 *Phys. Plasmas* **17** 056111
- [2] Kobayashi M *et al* 2013 *Nucl. Fusion* **53** 093032
- [3] Evans T E *et al* 2004 *Phys. Rev. Lett.* **92** 235003
- [4] Moyer R A *et al* 2005 *Phys. Plasmas* **12** 056119
- [5] Hudson B *et al* 2010 *Nucl. Fusion* **50** 045006
- [6] Evans T E *et al* 2008 *Nucl. Fusion* **48** 024002
- [7] Canik J M *et al* 2010 *Nucl. Fusion* **50** 064016
- [8] Suttrop W *et al* 2011 *Phys. Rev. Lett.* **106** 225004
- [9] Suttrop W *et al* 2011 *Plasma Phys. Control. Fusion* **53** 124014
- [10] Jeon Y M *et al* 2012 *Phys. Rev. Lett.* **109** 035004

- [11] Kirk A *et al* 2013 *Plasma Phys. Control. Fusion* **55** 015006
- [12] Kirk A *et al* 2013 *Nucl. Fusion* **53** 043007
- [13] Liang Y *et al* 2010 *Nucl. Fusion* **50** 025013
- [14] Liang Y *et al* 2013 *Nucl. Fusion* **53** 073036
- [15] Liu Y *et al* 2011 *Nucl. Fusion* **51** 083002
- [16] Brunzell P R *et al* 2004 *Phys. Rev. Lett.* **93** 225001
- [17] Drake J R *et al* 2005 *Nucl. Fusion* **45** 557–64
- [18] Paccagnella R *et al* 2006 *Phys. Rev. Lett.* **97** 075001
- [19] Martini S *et al* 2007 *Nucl. Fusion* **47** 783–91
- [20] De Bock M F M *et al* 2008 *Nucl. Fusion* **48** 015007
- [21] Frassinetti L *et al* 2010 *Nucl. Fusion* **50** 035005
- [22] Frassinetti L *et al* 2012 *Nucl. Fusion* **52** 103014
- [23] Frassinetti L *et al* 2014 *Plasma Phys. Control. Fusion* **56** 104001
- [24] Sun Y *et al* 2010 *Plasma Phys. Control. Fusion* **52** 105007
- [25] Dexter R N *et al* 1991 *Fusion Technol.* **19** 131
- [26] Escande D F *et al* 2000 *Phys. Rev. Lett.* **85** 1662
- [27] Marrelli L *et al* 2002 *Phys. Plasmas* **9** 2868
- [28] Lorenzini R *et al* 2008 *Phys. Rev. Lett.* **101** 025005
- [29] Bergerson W F *et al* 2011 *Phys. Rev. Lett.* **107** 255001
- [30] Lorenzini R *et al* 2009 *Nat. Phys.* **5** 570
- [31] Chapman B *et al* 2012 *EX/P6-01 Proc. IAEA Conf.*
- [32] Sarff J S *et al* 2013 *Nucl. Fusion* **53** 104017
- [33] Hegna C C 1996 *Phys. Plasmas* **3** 4646
- [34] Zanca P *et al* 2001 *Phys. Plasmas* **8** 516
- [35] Fitzpatrick R and Zanca P 2002 *Phys. Plasmas* **9** 2707
- [36] Fitzpatrick R *et al* 1999 *Phys. Plasmas* **6** 3878
- [37] Chapman B *et al* 2004 *Phys. Plasmas* **11** 2156
- [38] Reusch J A *et al* 2008 *Rev. Sci. Instrum.* **79** 10E733
- [39] Holly D J, Almagri A F, McCollam K J, Sarff J S and Tharp T D 2005 *Bull. Am. Phys. Soc.* **50** 39 <http://meetings.aps.org/link/BAPS.2005.DPP.BP1.39>
- [40] Tharp T D, Almagri A F, Chapman B E, Holly D J, McCollam K J and Sarff J S 2005 *Bull. Am. Phys. Soc.* **50** 37 <http://meetings.aps.org/link/BAPS.2005.DPP.BP1.37>
- [41] Holly D J and Dexter R N 1989 The spatial transform processor (internal report)
- [42] Hansen A K *et al* 1998 *Phys. Plasmas* **5** 2942
- [43] Terry P W and Whelan G G 2014 *Plasma Phys. Control. Fusion* **56** 094002
- [44] Sarff J S *et al* 1994 *Phys. Rev. Lett.* **72** 3670
- [45] Chapman B *et al* 2002 *Phys. Plasmas* **9** 2061
- [46] Sarff J S *et al* 2003 *Plasma Phys. Control. Fusion* **45** A45770
- [47] Hansen A K 2000 Kinematics of nonlinearly interacting MHD instabilities in a plasma *PhD Thesis*
- [48] Bartimoro R *et al* 1999 *Phys. Rev. Lett.* **83** 1779
- [49] Zanca P *et al* 2007 *Nucl. Fusion* **47** 1425–36
- [50] Ortolani S and the R F 2006 *Plasma Phys. Control. Fusion* **48** B371–81
- [51] Loarte A 2001 *Plasma Phys. Control. Fusion* **43** R183–224
- [52] Martines E *et al* 2010 *Nucl. Fusion* **50** 035014